Tellus (1988), *40A*, 1–25

A comparison of various normal-mode initialization schemes and the inclusion of diabatic processes

By RONALD M. ERRICO and PHILIP J. RASCH, *The National Center for Atmospheric Research, Boulder, Colorado 80307, USA*

(Manuscript received January 7, 1986; in final form February 27, 1987)

ABSTRACT

The field changes produced by various normal mode initialization schemes are compared. Dynamically balanced data are obtained from a climate simulation using a forecast model. The data are first degraded by a linear initialization, and then a nonlinear initialization is used in an attempt to recover the original fields. The nonlinear initializations include both diabatic and adiabatic schemes, applied to various sets of modes defined using both equivalent depths and natural periods as criteria.

Results indicate that diabatic initialization improves specification of the meridional mass streamfunction (i.e., the zonal wavenumber zero Hadley circulation) compared with adiabatic initialization. However, for zonally varying fields, the difference is less dramatic. An exception occurs when shallow modes are initialized, in which case near-surface fields are better specified using diabatic initialization. Errors in the tropical divergent wind field are typically half their true value, for either diabatic or adiabatic initializations. For vertical modes 1–2, errors in specification of mode coefficients are typically less than 20% of their true r.m.s. values. For shallower modes whose natural periods are less than one day, these errors are greater than 40%, but for those longer period modes, errors are greater than 80%.

The prognostic equation for a single mode coefficient is examined. Results suggest that, for medium depth, large horizontal scale tropical modes, a significant error source is the balance condition itself. For these modes, the time scales of their diabatic forcing, observed behavior, and natural (linear) behavior are all similar. In this case, the tendency term in the equations is not negligible.

1. Introduction

The body of knowledge surrounding nonlinear normal mode initialization (nonlinear NMI) has expanded steadily since the original work of Baer (1977) and Machenhauer (1977). However, there are several aspects which remain poorly understood. These problem areas result in subtle, but important variations in the way NMI is applied, and consequently in the data which are determined from NMI application. In this paper we analyze two of these poorly understood areas. We examine the sensitivity of the initialized data to the sets of modes and the terms (forces) which are included in the initialization.

The present study is a continuation of the works of Errico (1984) and Rasch (1985). Its purpose is to determine how well various nonlinear normal mode initialization schemes describe realistically balanced fields. The balanced fields are generated from an extended forecast so as to allow time for the model to dynamically adjust itself. The data are then degraded by first performing a linear initialization on all those gravitational modes to be initialized. Thus the projection of the degraded data contains neither phase nor amplitude information for those modes. The initializations are then used in an attempt to reproduce the original values of coefficients of those modes removed from the data. Various measures are used to quantify how well the coefficients or corresponding fields have been reproduced. This study is similar to those of Puri (1983, 1985), although comparisons range over a much wider set of NMI configurations, and different comparison methods are used, leading to different interpretations of the results of diabatic initializations.

Originally, in nonlinear normal mode initialization, the selections of modes were specified solely in terms of equivalent depths. All the gravitational modes whose equivalent depths were greater than some value were initialized (Williamson and Temperton, 1981). More recently, Puri and Bourke (1982) have discussed using the modes' natural frequencies as an additional criteria. Only those gravitational modes whose natural periods were less than some value (e.g., 48 hours) and whose equivalent depth lay within the correct subset were initialized. Some of the issues regarding the choice of modes for the initialization have been examined in more detail in Puri (1983, 1985), Errico (1984), and Rasch (1985).

The question of which terms (forces) should be included in the normal mode balance condition has also been inadequately addressed. In its early applications, only adiabatic terms were considered in NMI because Machenhauer's iterative scheme (Machenhauer, 1977), which was used to solve the appropriate nonlinear equations, failed to converge when diabatic terms were included. However, it was soon observed that when tropical internal modes were initialized, the tropical circulation (e.g., the Hadley cell) was considerably weakened. This weakening was recognized as a consequence of the corresponding weakness of the adiabatic nonlinear (i.e., advective) forcing of the tropical modes (Bengtsson, 1981). Since the dominant forcing in the tropics is diabatic (convective and radiative), it was considered relevant to incorporate diabatic terms in the normal mode balance condition (Bengtsson, 1981; Kitade, 1983; Wergen, 1983). Kitade suggested the use of an under-relaxation scheme to improve the convergence problems. Wergen used a diabatic forcing field that was fixed so as to not affect convergence of Machenhauer's scheme. More recently, Rasch (1985) developed an iterative scheme with better convergence properties. In his scheme, diabatic effects and shallow modes (which also created convergence problems in the other NMI schemes) were included.

The questions of which modes to initialize and how to initialize them have many aspects that require careful consideration. Which modes are actually in a state of balance in the atmosphere? How noisy is the forecast and what modes are causing the noise? What problems, if any, are caused by the noise (i.e., how important is elimination of the noise)? How inaccurate is the analysis? Are some fields so poorly analyzed (e.g., tropical divergence) that educated guesses would be more appropriate than analyses? Not only must these questions be answered, but the impact of initializations on model forecasts must be examined as well.

The question of which modes are balanced in the atmosphere is perhaps the most difficult to answer. The fields simply cannot be measured with sufficient accuracy. If that were not the case, initialization would likely be unnecessary. However, it is not difficult to determine which modes tend to be balanced within a model simulation due to the model's own dynamic adjustment. Such a determination is relevant for many reasons. In this context, both fields and forces are known precisely. A model must be used in any case, since the quantitative determination of forces used in the initialization requires a model context. Even if the model balance is different from that of the atmosphere, it is important to investigate the model balance in its own respect. Any difference between model and atmospheric balances will likely be interpreted as an imbalance by the model, and will therefore tend to create noise if the model is initialized with a balance condition appropriate only for the atmosphere. Model balance has been investigated by Errico (1984) for the Community Forecast Model (CFM; also called CCM0B) at the National Centre for Atmospheric Research (NCAR).

Since a model simulation is used in place of observed atmospheric data, some results may not apply to the atmosphere. Significant errors exist in models used for research (e.g., see Krishnamurti, 1983) and operational forecasting (e.g., see Kanamitsu (1985) or Heckley (1985)). However, the observed data are also poor quality (see Section 9 for further discussion and references), so it is not even a simple problem to quantify the model errors. The extent to which results of this study are applicable to other models or the atmosphere is therefore uncertain. The results are explained using simple physical arguments, but these arguments require assumptions or sufficient knowledge of atmospheric forcing characteristics. This study also presents a method of investigation for similar studies with other models, so that the question of generality may be answered.

It is difficult to meaningfully present how well each scheme performs using relatively few numbers. Many measures tend to be misleading and are easily interpreted incorrectly. For example, comparisons of zonal-mean meridional stream functions only reveal differences in one wave number, the zonal mean. Examination of total wind errors (rotational plus divergent) can be misleading because such differences are likely to be small with respect to the total wind field (since only a small portion of the total is affected by the initializations). Contour plots of velocity potential, which have often been used in similar studies (e.g., Puri, 1985), emphasize the largest scales of divergent motion. The physically meaningful velocities derived from them depend on structural details which are difficult to perceive in such plots. This is discussed further in the Appendix.

For historical reasons, we have used zonal-mean meridional streamfunctions to provide an estimate of the instantaneous Hadley circulation. However, rather than presenting figures of velocity potential, the corresponding figures of differences in the divergent component of velocity will be presented. The divergent component is chosen since it is expected to change more than the rotational component when initialized. Changes in the mode coefficients themselves also will be examined.

Table 1. *The nine σ-levels in the model, the basic state temperatures at those levels, used to determine the normal modes, and the resulting equivalent depths, ordered largest to smallest*

l	σ	$\bar{T}(K)$	$H(m)$
1	0.009	218.15	9816.34
2	0.074	218.15	3511.59
3	0.189	218.15	657.08
4	0.336	233.54	146.73
5	0.500	251.89	45.94
6	0.664	265.87	15.15
7	0.811	276.19	4.94
8	0.926	283.25	1.27
9	0.991	286.93	0.18

The model and data used for this study are described in Section 2. Details of the various NMI schemes are presented in Section 3. Methods of data comparison using meridional stream functions, divergent winds, and normal mode coefficients are described in Section 4. Results using these three methods are presented in Sections 5–7, respectively, with summaries at the end of each section. A simple model and its solutions are described in Section 8 for the purpose of explaining the results obtained with the complete general circulation model. Finally, the results are discussed and conclusions presented in Section 9.

2. Model and data

The model used to create the balanced fields and to compute the nonlinear terms for the initialization is the NCAR CFM (Williamson, 1983). It is a spectral model with rhomboidal truncation at wave number 15. The vertical coordinate is σ (pressure at level, divided by surface pressure), with data specified on nine discrete levels. Physical processes include surface drag and surface fluxes of temperature and moisture, moist and dry convective adjustment, horizontal and vertical diffusion, and solar and infrared radiation (Ramanathan et al., 1983).

January and July datasets were used in this study. The January dataset is from day 75 of a perpetual January climate simulation. This dataset is included in those examined in Errico's (1984) analysis of balance in the CFM. The July dataset is from day 180 of a perpetual July climate simulation. These times are sufficiently long so that the model's natural dynamic balance has been obtained (irrespective of reasonable initial conditions; Errico, 1984).

The normal modes used for initialization of these datasets are defined using the CFM equations, linearized about a state of rest, with a temperature $\bar{T}$ varying only in σ. The CFM σ levels, corresponding values of $\bar{T}$, and a list of equivalent depths for the nine vertical modes appear in Table 1. The structures of the vertical modes corresponding to the four largest equivalent depths appear in Fig. 1.

The actual structures and frequencies of the initialized modes may depend strongly on the

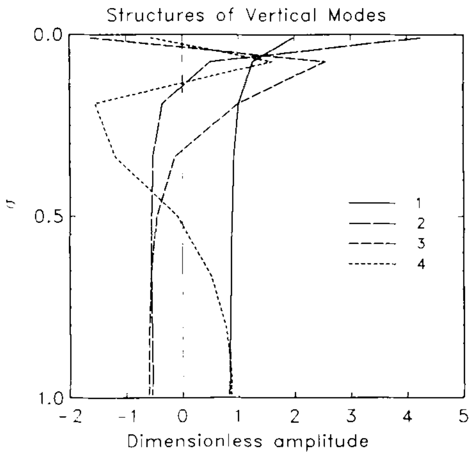

Fig. 1. The first four vertical structure functions used for initialization of the NCAR CFM.

choice of basic state around which the model is linearized. At most operational centers, the basic state chosen is similar to the one here, especially with regard to it being one of rest. Since such a linearization ignores the strong effects of zonal advection, the determined modes will be unrealistic with regard to both the atmosphere and the complete model. The effects of such advection are considered by the initialization as nonlinear terms. However, although they are not ignored by the initialization, it may be that the sets of modes which are initialized are not the proper sets because the modes are not the true modes. Unfortunately, determination of modes for more realistic basic states was not possible for this study. Neither was it appropriate, since one intention was to compare current operational, nonlinear normal-mode initialization schemes.

3. Initialization methods

In this section we define the various initialization methods tested in later sections. The initialization configurations are summarized in Table 2.

Each dataset produced by the various initialization procedures is compared with the pre-initialized dataset (denoted TRUTH). TRUTH is considered dynamically adjusted, consistent with the model's own dynamic and diabatic processes (Errico, 1984).

Linear normal mode initialization is used to degrade the data. The resulting dataset is denoted by LIN. The procedure requires determination of the complex coefficients of modes of all selected scales for the dataset in question. The projections of these modes are then subtracted from the data. The resulting data are degraded in the sense that the coefficients of all selected modes are zero. Therefore, the degraded data contain no direct information regarding the original amplitudes or phases of the modes to be initialized. However,

Table 2. *Initialization configurations (see text for more detail)*

TRUTH	Datasets taken from long runs of the model for perpetual January and July simulations, for which a true model balance has been attained.
LIN	A linear initialization of a TRUTH type dataset.
ADIAB	An adiabatic initialization of a LIN type dataset.
DIAB	A diabatic initialization of a LIN type dataset.
DIAB-T	A diabatic initialization of a TRUTH type dataset.
FIXE-T	An initialization of a LIN type dataset, using a heating field which projects on modes with periods greater than 11 hours. The heating field is that arising from the time average of a 2-hour integration of a TRUTH type dataset.
FIXE-D	An initialization of a LIN type dataset, using a heating field which projects on modes with periods greater than 11 hours. The heating field is that arising from the time average of a 2-hour integration of a LIN type dataset.
FIXN-T	An initialization of a LIN type dataset, using a heating field which projects on all modes included in the initialization. The heating field is that arising from the time average of a 2-hour integration of a TRUTH type dataset.
FIXN-D	An initialization of a LIN type dataset, using a heating field which projects on all modes included in the initialization. The heating field is that arising from the time average of a 2-hour integration of a LIN type dataset.

for some modes, that information can be determined from the degraded data by indirect means, e.g., by nonlinear initialization.

For all the nonlinear NMI configurations, we have used the Machenhauer (1977) condition that the time tendencies of the coefficients vanish for a set of selected modes. Solution of the numerous, coupled nonlinear equations requires use of an iterative, numerical scheme. Rasch's (1985) scheme is used here because it has better convergence properties than Machenhauer's (1977) scheme. In particular, iterations with Rasch's scheme converge in cases which include diabatic processes and modes with small equivalent depth, whereas iterations with Machenhauer's scheme do not. In configurations where iterations with both schemes converge well, they yield almost identical solutions.

Five iterations of Rasch's scheme were performed (the first iteration is that after the initial Machenhauer step; Rasch, 1985) with no underrelaxation. Five iterations were chosen since then the results are relatively iteration independent. Actually, most of the changes due to initialization occur by the second iteration as shown by Rasch (1985), although he used underrelaxation which further slowed convergence. Therefore, the results are not significantly different from those that would have been obtained if only two iterations had been performed.

In this study, particular sets of modes to be initialized are selected using only the criteria of equivalent depth (i.e., vertical scale, denoted by index l), resonant time scale T (i.e., the period determined from the eigenvalue corresponding to each mode), and mode type (only gravitational). Only four sets are considered. The smallest set contains all gravitational modes with $l \leqslant 4$ and $T \leqslant 24$ hours. This set is denoted 4V-24T. Another set includes all 9 vertical modes with $T \leqslant 20$ hours (denoted 9V-20T). This set is chosen because it includes most of those modes which are dynamically balanced in the CFM, as reported by Errico (1984). The remaining sets, denoted 4V-48T and 4V-allT, are chosen because they are similar to the sets initialized operationally at the National Meteorological Center (NMC) and the European Center for Medium Range Weather Forecasts (ECMWF), respectively.

All the nonlinear initializations include all the model's adiabatic terms. If only such terms are included, the initialization is called adiabatic, denoted as ADIAB. In some initializations, all diabatic terms are also included, with their evaluation every iteration, consistent with the data for that iteration. This type of initialization is denoted by DIAB, and is made possible by Rasch's (1985) scheme.

Prior to the use of Rasch's (1985) scheme, it was necessary to hold the diabatic terms fixed during iteration with Machenhauer's (1977) scheme. At ECMWF, Wergen (1983) specified these fixed values by producing a three-hour forecast starting from the non-initialized data analysis, evaluating the time-averaged diabatic heating during the last two hours, and smoothing the result by only applying the heating to gravitational modes with $T > 11$ hours. This initialization method is denoted by FIXE. A similar method, but without the smoothing of the heating fields, has been applied by Ballish (personal communication) at NMC. This method is denoted by FIXN.

Due to computational considerations, the FIXN and FIXE initializations have not been performed exactly as done at either NMC or ECMWF. As applied in this study, all configurations use Rasch's (1985) scheme. All the diabatic processes of the model are included in the forecasts used to compute the time-mean diabatic heating. However, in the FIXE and FIXN initializations, the only diabatic heating explicitly considered is that due to moist and dry convective adjustment and to condensational heating in dynamically stable layers. In other words, only those processes are considered in the calculation of the time-mean heating field, although all model processes contributed to produce those fields. Particularly excluded in the calculation of the time-mean are momentum drag (included at NMC), surface heat fluxes (included at both NMC and ECMWF), and vertical and horizontal diffusion of temperature and momentum, which are all diabatic terms in the CFM. Except near the surface, these neglected diabatic terms are small compared with convective heating (Errico, 1984).

The heating fields used in the FIXN and FIXE type NMIs depend upon whether the integration used in the time averaging of the heating proceeds from a perfect set of initial conditions, or from the degraded data. In an attempt to bracket the possible sensitivity of the NMIs to the heating, both types of fixed heating have been used. For these configurations, the suffix "T" implies the heating fields were computed from TRUTH, while those with a "D" suffix imply the heating fields were computed from the degraded dataset LIN.

DIAB type initializations have been made using both TRUTH (denoted DIAB-T) and LIN (denoted DIAB; no suffix) as the starting values in the iteration scheme. In some sense DIAB-T is the most promising candidate for a "best possible" NMI scheme, since the nonlinear terms (both adiabatic and diabatic) are identical to the TRUTH for the initial iteration. All errors in the data which result from the initialization are due to errors in the assumed (Machenhauer) balance condition and the errors introduced in subsequent iterations.

Actually, the differences between the instantaneous heating field and the time averaged heating from TRUTH are quite small, whereas the time averaged heating rate from LIN differs significantly. For the scales resolved by our model, the latent heat release by moist convective adjustment and large scale stable condensation dominate the heating terms. At $\sigma = 0.5$, heating rates are as large as 50 K/day at discrete gridpoints in the model when the model is in balance. These maxima are reduced by a factor of four however when the heating field is truncated to the R15 resolution of the model. Fig. 2a shows the truncated instantaneous heating, 2b the time averaged heating fields from TRUTH, and 2c the time averaged heating from LIN. The first two fields both show maxima of about 12 K/day, and differ by less than 1 K/day except in the region just north of Madagascar (about 6 K/day), and along the northeast coast of South America (3 K/day). The time averaged heating determined from the LIN dataset is much weaker. The heating rates are all less than 1 K/day, except over the northeast coast of South American where the maxima is nearly 4 K/day.

4. Comparison methods

Differences between TRUTH and any initialized dataset are due to combinations of several causes. These causes include initializing modes which the model itself does not tend to balance, excluding terms which are important in the balance, or using an inappropriate initialization condition (Machenhauer's (1977) condition is necessarily approximate). Whatever the cause, the comparisons indicate how well a particular procedure reproduces a simulated atmospheric balance.

The first method of comparison is determination of the zonal-mean meridional mass stream functions ψ for each dataset. These are often presented for comparisons of normal mode initialization schemes (Rasch, 1985; Puri, 1983, 1985; Kitadi, 1983; Wergen, 1983). The circulation described is commonly called the Hadley Circulation, although strictly speaking, it describes only part of it (Lorenz, 1967). The ψ are determined from zonal-mean fields of either the northward wind component $\bar{v}$ or the substantial derivative of pressure with respect to time, $\bar{\omega}$, such that

$$g\frac{\partial\psi}{\partial p} = \bar{v}2\pi a \cos\phi, \tag{4.1}$$

$$g\frac{\partial\psi}{\partial\phi} = -\bar{\omega}2\pi a^2 \cos\phi, \tag{4.2}$$

where g is the acceleration of gravity, ϕ is latitude, p is pressure, a is the earth's radius, and an overbar here denotes a zonal mean value. Since ψ is determined from only zonal mean fields, it only depends on normal modes of zonal wavenumber $m = 0$. This is a small subset of the total number of gravitational modes. Since these modes are rather peculiar compared to zonal-varying gravitational modes (Kasahara, 1978), conclusions based on comparisons of ψ are not generalizable to zonally-varying fields.

The second method of comparison is the determination of the magnitude of the divergent wind V_d and the magnitude of its difference ΔV_d. These are evaluated as

$$V_d = (u_d^2 + v_d^2)^{1/2} \tag{4.3}$$

$$\Delta V_d = ((\Delta u_d)^2 + (\Delta v_d)^2)^{1/2} \tag{4.4}$$

where u is the eastward wind component, and the subscript d refers to the divergent portion. The divergent portion is determined using global spectral transforms consistent with the model truncation (Machenhauer, 1979). Since the differ-

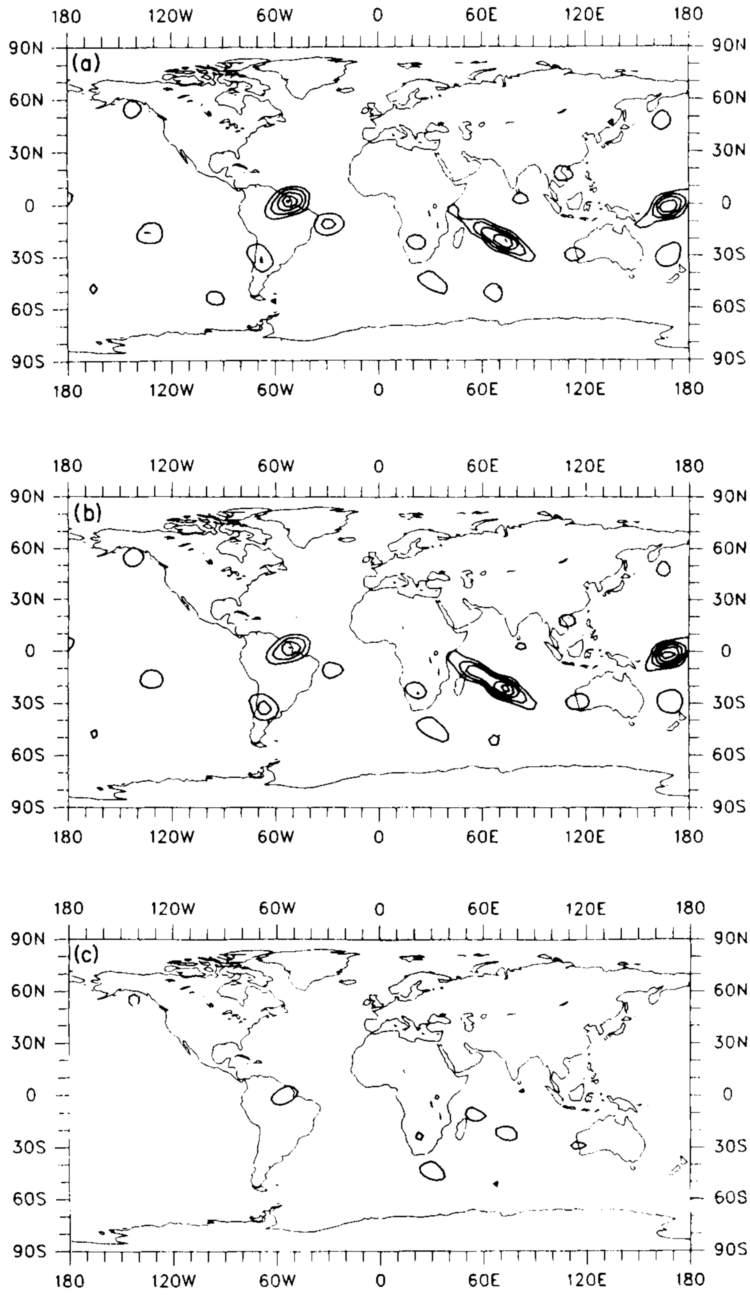

Fig. 2. The spectrally truncated heating field used for the January initializations at $\sigma = 0.5$. (a) The instantaneous heating field of dataset TRUTH. (b), (c) The two-hour time-mean heating fields determined from forecasts starting from TRUTH and LIN, respectively. Contour interval 2 K/day.

ences Δu and Δv between datasets are computed before squaring and summing, ΔV_d includes differences due to speed as well as direction. Fields of ΔV_d were particularly chosen because gravitational modes describe most of V_d, but little of the rotational wind component. Also, V_d is an important field for determining the local heating since it determines ω and the horizontal moisture convergence.

Typically in initialization studies, fields of velocity potential χ are presented for non-initialized and initialized datasets. This χ satisfies

$$\frac{\partial \chi}{\partial \vartheta} = u_d a \cos \phi, \qquad \frac{\partial \chi}{\partial \phi} = v_d a, \tag{4.5}$$

where ϑ is the longitude. We find comparison of fields of χ often misleading, especially in the context of initialization. Since χ is determined by a spatial integral of the u_d and v_d fields, it tends to emphasize larger scales and to de-emphasize smaller scales. The physically meaningful fields of u_d and v_d are determined by the gradient of χ; i.e., by the spacing of contours and wiggles in χ, and not by the overall pattern of χ that the eye tends to see. Also, for the reader to compare by eye, it is more appropriate to present figures of differences, rather than figures of pairs of fields themselves. For these reasons, fields of ΔV_d rather than χ are presented in this study.

The third comparison method is determination of the differences in modal coefficients as determined from the datasets to be compared. The coefficients are determined by simple projection of the data onto the modes. In all cases, the differences are presented as square roots of normalized variances, denoted by R_l, and defined by

$$R_l = \left[\frac{\sum_{J \in S} |\Delta c_{J,l}|^2}{\sum_{J \in S} |c_{J,l}|^2} \right]^{1/2}, \tag{4.6}$$

where $c_{J,l}$ is the coefficient of a particular mode denoted by indices J and l, vertical bars indicate the modulus of a complex number, Δ denotes a difference between coefficients determined from different datasets, and the sums are over a set of modes S, all of which have the same vertical mode index l. The coefficients in the denominator are determined from the non-initialized dataset TRUTH. The quantity $|c|^2$ equals the kinetic plus available potential energy contributed by the denoted mode. (Actually this is true only if one vertical mode is present in the data, since the vertical modes here are not strictly orthogonal. However, it is a good approximation for $l = 1, \ldots, 4$ since these vertical modes are very nearly orthogonal.) Therefore R_l accounts for differences in temperature, surface pressure, rotational and divergent winds. Normalized as it is, a value of 1 indicates that the errors in the coefficients determined from the NMI are as large as the TRUTH coefficients themselves; i.e., the initialization shows no skill.

5. Analyses of meridional stream functions

The ψ field for the January TRUTH is presented in Fig. 3a. The circulation about the maximum value is clockwise. The ψ field after a LIN 4V-48T initialization is presented in Fig. 3b. That field is approximately 30% weaker, judging from the maximum value of ψ. This weakening of the zonal-mean circulation indicates that those $m = 0$ gravitational modes which are included in the initialized set describe a significant portion of that circulation. The ψ field after an ADIAB 4V-48T initialization is presented in Fig. 3c. It is qualitatively similar to ψ obtained from linear initialization. This similarity indicates that the adiabatic nonlinear terms which are used to balance the $m = 0$ modes in the 4V-48T set are themselves small. The ψ field after a DIAB 4V-48T initialization appears in Fig. 3d. Diabatic initialization results in a circulation that is 15% stronger than the original, non-initialized circulation. Qualitatively similar results are obtained for the July dataset.

The field of ψ obtained from initializing the January dataset using the scheme FIXN-T 4V-48T is presented in Fig. 3e. The intensity of the resulting ψ field is between those of TRUTH and ADIAB 4V-48T. This improvement is explained in Section 8. The ψ field which results from a FIXE-T 4V-allT initialization is presented in Fig. 3f. The mean meridional circulation is not much stronger than that obtained from the ADIAB 4V-48T initialization.

In an operational setting, the heating field that corresponds to TRUTH is not known, because

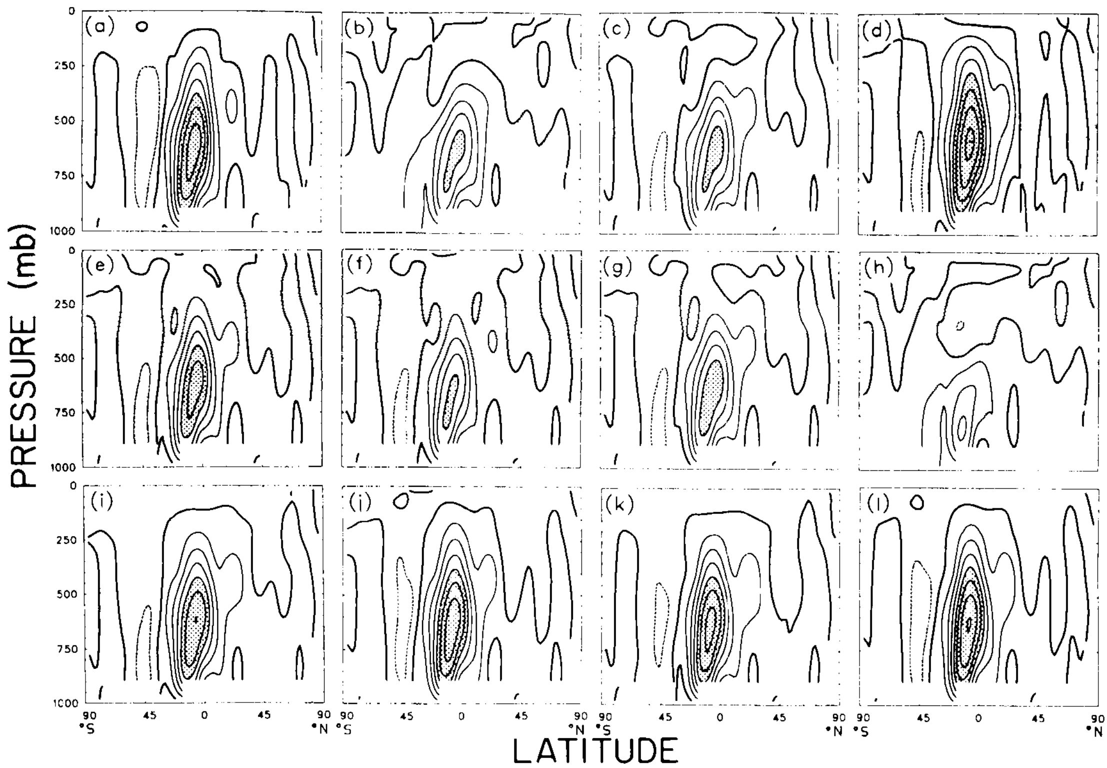

Fig. 3. The meridional streamfunctions for the January dataset following various initializations. Contours are in units of 5×10^{10} kg s^{-1}. Light stippling denotes region less than -5×10^{10} kg s^{-1}. Heavy stippling denotes regions greater than 20×10^{10} kg s^{-1}. (a) TRUTH, (b) LIN 4V-48T, (c) ADIAB 4V-48T, (d) DIAB 4V-48T, (e) FIXN-T 4V-48T, (f) FIXE-T 4V-allT, (g) FIXN-D 4V-48T, (h) LIN 4V-allT, (i) ADIAB 4V-24T, (j) LIN 4V-24T, (k) ADIAB 9V-20T, (l) DIAB 9V-20T.

the data analysis has errors and the parameterizations of heating are imperfect. Therefore the ψ field which results from an FIXN-type initialization which uses a degraded diabatic heating field is presented in Fig. 3g (FIXN-D 4V-48T). The heating so obtained is weaker than in the former case, since the initial degraded divergence field is considerably weaker after linear initialization. The resulting ψ field is in this case similar to that produced by adiabatic initialization. The sensitivity of diabatic initialization to the prescribed heating field has been described by Puri (1985). When the degraded heating is used, the FIXE 4V-allT initialization also produces a weaker circulation (not shown).

The FIXE 4V-allT initializations with either correct or degraded heating produce weaker ψ fields than do the corresponding FIXN 4V-48T initializations. The 4V-allT initializations have a disadvantage in these comparisons. Since the set of modes to be initialized is larger, there is more likelihood of an incorrect determination of some modal amplitudes. The ψ field for the linearly initialized, 4V-allT January dataset is presented in Fig. 3h. It is much weaker than that corresponding to LIN 4V-48T (Fig. 3b). The slow, large scale modes, which are included in the former set, but not in the latter, describe a major portion of the tropical circulation (including the Hadley circulation) as described by Puri (1983). The poorer results obtained with the FIXE initializations as compared to those of FIXN demonstrate that these modes are not dynamically balanced in the CFM, in agreement with Errico's (1984) analysis of the CFM's balance.

The ψ field which results from an ADIAB 4V-

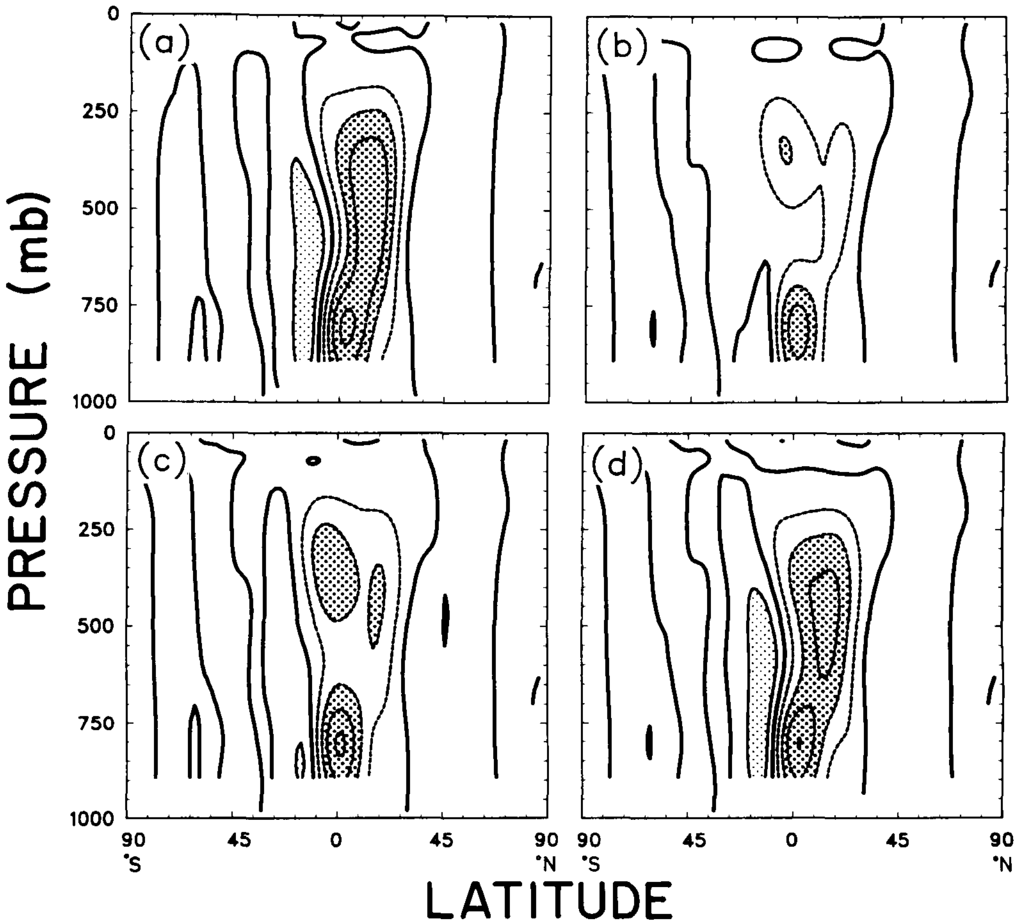

Fig. 4. The meridional streamfunctions for the July dataset. As in Fig. 3 except: Heavy stippling denotes regions less than -10×10^{10} kg s^{-1}. Light stippling denotes regions greater than 5×10^{10} kg s^{-1}. (a) TRUTH, (b) LIN 4V-48T, (c) FIXN-T 4V-48T, (d) ADIAB 4V-24T.

24T initialization of the January dataset is presented in Fig. 3i. It is only slightly weaker than the TRUTH field. A DIAB 4V-24T initialization (not shown) produces a ψ field which is slightly stronger than the TRUTH field. The two 4V-24T initializations produce better ψ fields because the 24T cutoff restricts the initialization changes to a smaller set of modes. This is revealed by examination of ψ after a 4V-24T linear initialization, as presented in Fig. 3j. Even that initialized field closely resembles the TRUTH field, indicating that the ψ field is dominated by modes whose periods are longer than 24 hours.

ADIAB or DIAB initializations of the set 9V-20T (Figs. 3k, l respectively) produce ψ fields still closer to the TRUTH. For these last two cases, although more vertical modes are initialized, the period cutoff further restricts the initialized set of modes. These results agree with those of Puri and Bourke (1982) who state that a judicious use of a frequency cutoff will retain most of the ψ circulation. Of course, all of it may be retained by simply restricting the initialization to nonzonal modes. Then the initialized ψ will necessarily be identical to the non-initialized, or analyzed, ψ. However, if this non-initialized ψ is contaminated by errors, so that strong and rapid, zonal-mean gravitational oscillations occur in a subsequent forecast, then a forecast from datasets initialized in this way will also have such oscillations.

The ψ field determined for the July dataset (TRUTH) is presented in Fig. 4a. Compared with that for the January dataset (Fig. 3a), the sign is changed (the circulation is reversed) and the amplitude is nearly halved. The ψ field resulting from an ADIAB 4V-48T initialization of the July dataset is presented in Fig. 4b. It bears little resemblance to the true ψ field. The ψ field resulting from a FIXN-T 4V-48T initialization appears in Fig. 4c. It has nearly the strength of the true ψ field, but the structure is significantly different. A DIAB 4V-48T initialization (not shown) also results in such a structure, but in that case the ψ field is over-amplified by 30%. The double-maxima structure appearing in Fig. 4c is dominated by the third and fourth vertical modes (Fig. 1), and therefore this structure is partly a consequence of the choice of four vertical modes for initialization. A similar double-maxima structure also appears in climatological studies of ECMWF operationally initialized data (Rosen and Salstein, 1985). The ψ field resulting from an ADIAB 4V-24T initialization, presented in Fig. 4d, also has this structure. However, as for the January case, such an initialization produces a field more like TRUTH because fewer modes are affected by the initialization. In other respects, the comments regarding the various initializations of the January dataset apply to those of the July dataset as well.

In summary, a significant portion of the ψ field can be altered by an initialization of four (or more) vertical modes with a period cutoff of 48 hours or more. If such an initialization is adiabatic, it considerably weakens ψ (Bengtsson, 1981), while a fully diabatic one strengthens it (Rasch, 1985). When applied to such modes, initializations which use some estimate of the diabatic heating as a fixed term in the iteration scheme produce ψ fields closer to the truth, but only if the heating is sufficiently correct (Puri, 1985). Finally, initializing fewer modes, such as with a shorter period cutoff, affects ψ less (Puri and Bourke, 1982). It must be remembered that these comments apply only to the zonal-mean $\bar{v}$ and $\bar{\omega}$ fields. Thus far, only a small portion of the total variance of the fields have actually been presented or discussed. A more comprehensive analysis of the total fields is presented in the remaining sections.

6. Analyses of divergent winds

The field of V_d for the January (TRUTH) dataset as a function of latitude and longitude at the 0.189 σ-level is presented in Fig. 5a. This σ-level is chosen because it is the level of maximum divergent wind. The strongest divergent winds are in the tropics, where most speeds are greater than 5 m/s. The maximum speed is 20.3 m/s over the Western Pacific Ocean. Other large values are 13.2 m/s over Peru, 18.0 over the Western Indian Ocean, and 16.2 over the Himalayan Mountains. Large values typically occur in regions of either steep orography or strong convective heating. Clearly, the divergence is forced in these regions.

The field of ΔV_d at the 0.189 σ-level, produced by comparing TRUTH and ADIAB 4V-48T for January, is presented in Fig. 5b. *Note that the shading here represents one-half of the values in 5a.* Significant values are restricted to the tropics. Even there, most values are less than half those of V_d for TRUTH. There are four regions of relatively large errors. All the regions of relatively large error are near regions of strong convective heating, although the two do not always coincide (compare with Fig. 2). The maximum error is 18.1 m/s, coinciding with the maximum V_d in the Western Pacific Ocean. Note that there is little relative error over mountains. Apparently, adiabatic initialization properly acounts for the effects of orography on divergence.

The field of ΔV_d at the 0.189 σ-level, produced by comparing TRUTH and FIXN-T 4V-48T for January, is presented in Fig. 5c. This particular initialization is chosen because it produces the least errors in the V_d field. There are again four regions of large error, although not colocated with those in Fig. 5b. The errors are generally smaller than in the previous case. In particular, the error in the Western Pacific Ocean of 10.9 m/s is nearly half the value of TRUTH. The fields of ΔV_c for the January FIXE-T 4V-allT case with correct heating, produced by comparison with TRUTH, are similar to those for the FIXN-T 4V-48T case, except values are typically 20% greater than with FIXE. This is likely due to the added difficulty of initializing more modes in the FIXE case than in the FIXN case. If the degraded diabatic heating is used in either of the two previous cases, the ΔV_d fields resemble those

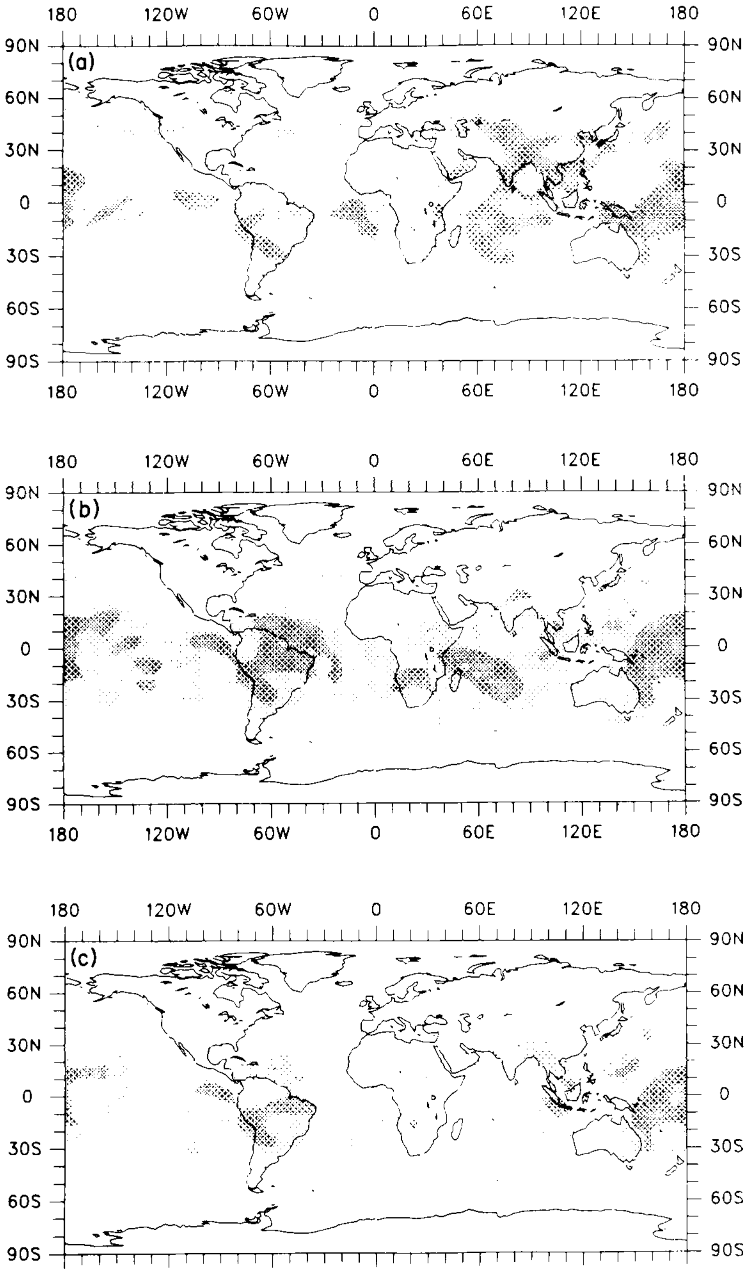

Fig. 5. The amplitude of the divergent wind component V_d for the January dataset at $\sigma = 0.189$. Light stippling implies amplitudes greater than 5 m s^{-1}. Heavy stippling implies amplitudes greater than 10 m s^{-1}. (b) ΔV_d for ADIAB 4V-48T, (c) ΔV_d for FIXN-T 4V-48T. Light stippling implies amplitudes greater than 2 m s^{-1}. Heavy stippling implies amplitudes greater than 4 m s^{-1}.

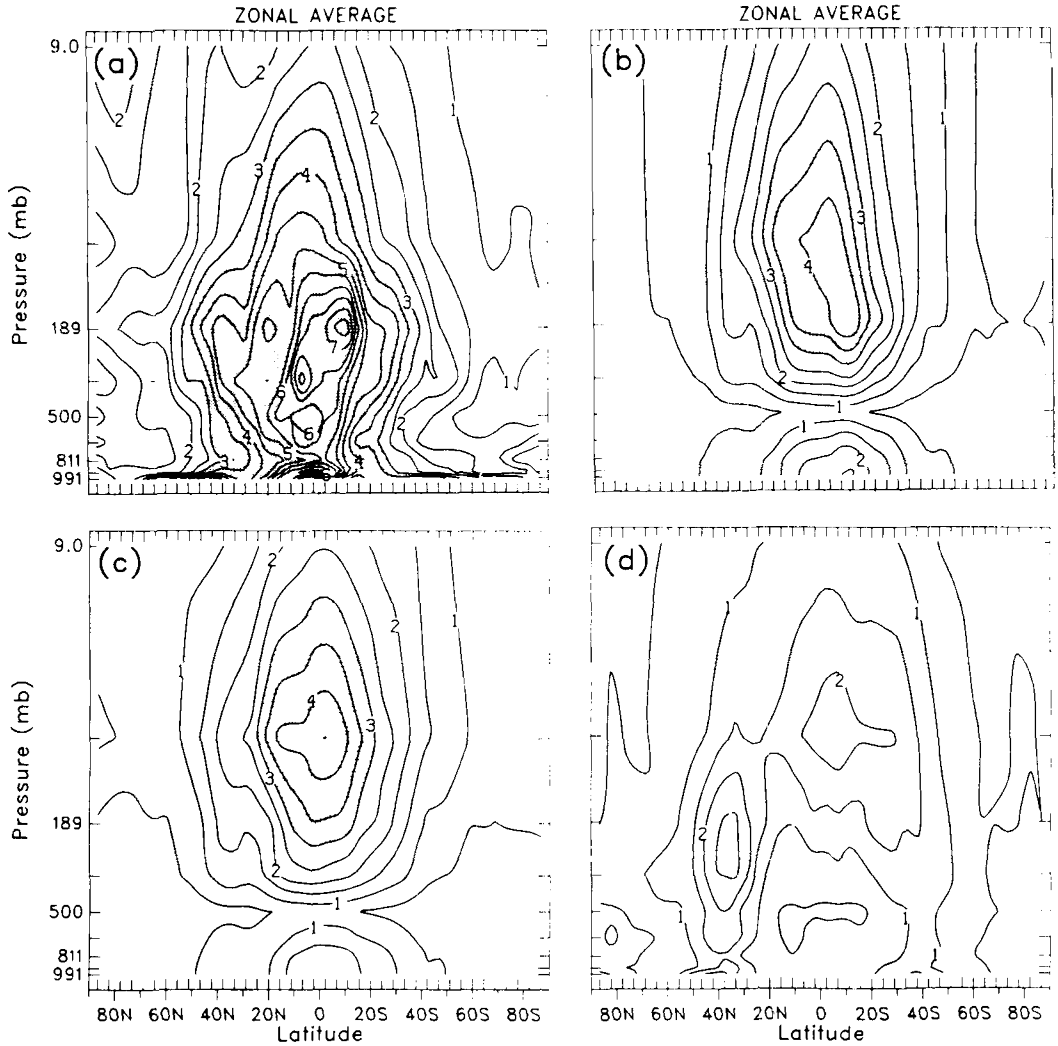

Fig. 6. (a) The zonal average of V_d for the January dataset. (b), (c), (d) The zonal average ΔV_d for the January dataset for initializations ADIAB 4V-48T, FIXE-T 4V-allT, and DIAB 9V-20T, respectively. Stippled areas imply amplitudes greater than 3 m s^{-1}. Values of σ corresponding to each level are presented in Table 1.

of the ADIAB 4V-48T case.

The zonally averaged field of V_d for January TRUTH is presented in Fig. 6a as a function of σ and latitude. The (zonally averaged) magnitude of the divergent wind is greatest near the tropical tropopause, although a nearly equal secondary maximum appears near the surface. Each of Figs. 6b–d is determined by comparing the initialized dataset with the January TRUTH.

The zonal-mean ΔV_d field produced from ADIAB 4V-48T appears in Fig. 6b. The maximum value is 4.47 m/s near the tropical tropopause. This is approximately 50% of the value of TRUTH. Outside the tropics, the error is typically 20%.

The zonal-mean ΔV_d field determined from the January FIXE-T 4V-allT initialization is presented in Fig. 6c. The maximum error is 4.51 m/s near the tropical tropopause. The zonal-mean ΔV_d field for the January, FIXN-T 4V-48T case (not shown) is qualitatively similar, except most values are approximately 15% smaller. In fact, the structures of the zonal-mean ΔV_d fields for all 4V-48T and 4V-allT initialized datasets are qualitatively similar. In particular, they all have maxima in the tropics near both the tropopause and the surface.

As an example of a qualitatively different error field, the zonal-mean ΔV_d for DIAB 9V-20T is presented in Fig. 6d. The error field is typically half as large as in Figs. 6b–c. The ΔV_d for ADIAB 9V-20T (not shown) is qualitatively similar, except in the lowest model σ-level, where values greater than 5 m/s occur. These large, near surface errors occur in the adiabatic, 9 vertical mode case because the actual model balance for the shallow modes is dominated by the diabatic surface drag (Errico, 1984; Ballish and Baer, 1985). The structures of the 9V-20T initializations are different from those in the previous figures both because more vertical modes are affected and because fewer modes are selected by the shorter period cutoff.

The divergent wind errors for several initializations are summarized in Figs. 7a–c. There, the errors are presented as global averages of ΔV_d as a function of σ-level.

In Fig. 7a, the initializations are all for the January dataset, applied to four vertical modes. Errors for the LIN 4V-allT and LIN 4V-48T initializations are provided for reference. Those initializations represent an extreme type of error with which to compare the errors from nonlinear initializations. Note that the errors with both LIN are similar, except errors from the allT initialization are approximately 10% larger at most levels. The errors from the ADIAB 4V-48T initialization are approximately half as large as the LIN 4V-48T errors at all levels. In other words, that adiabatic initialization recovers approximately half of the divergent wind field. The FIXN-T 4V-48T initialization produces the smallest errors at all levels. At low levels, these errors are approximately 25% less than the errors from the adiabatic case, but at high levels, the errors are only 10% less. Errors from the FIXE-T 4V-allT initialization are between those of the ADIAB and FIXN-T cases, except at high levels, where they are slightly worse than those of the ADIAB case. The errors from the FIXN and FIXE cases with the degraded heating are similar

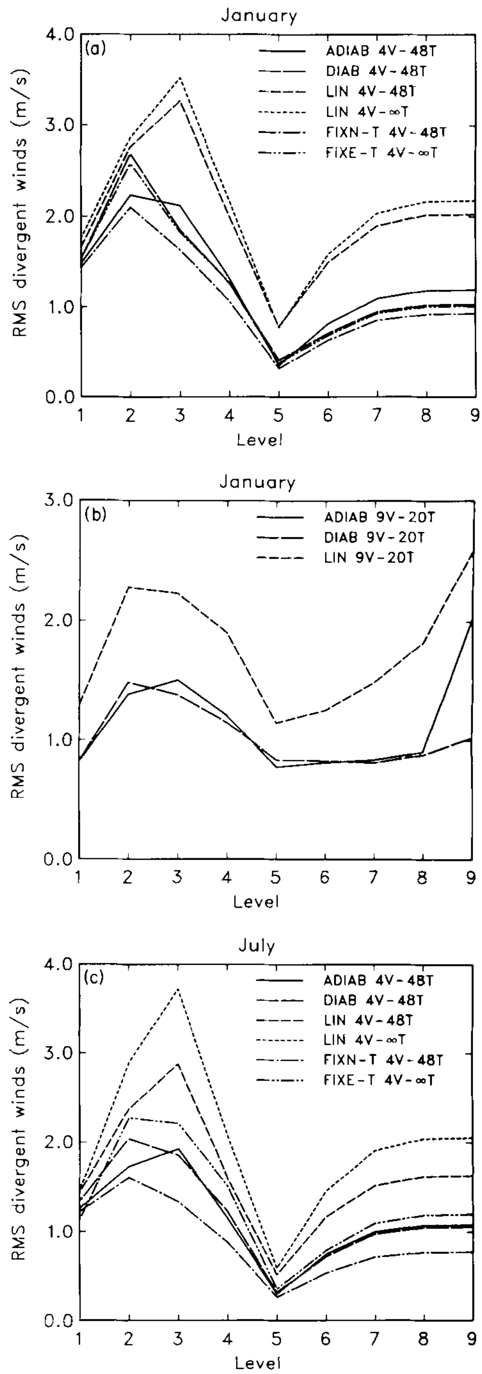

Fig. 7. Global averages on sigma levels of ΔV_d for the January initializations. (a) The four vertical mode initializations. (b) The nine vertical mode initializations. (c) As in Fig. 7a except for the July simulation.

to those of the ADIAB case. Note that errors for all the 4V cases are characterized by double maxima.

A summary of ΔV_d for the 9V-20T initializations of the January dataset appears in Fig. 7b. As for the cases in the previous figure, the nonlinear initializations recover approximately half of the divergent wind field at intermediate levels. Two new pieces of information are in this figure. When the period cutoff excludes most large-scale tropical modes, as with 20T, the differences between a diabatic and adiabatic initialization are small at most levels. An exception occurs when the shallowest vertical modes (e.g., all nine, as here) are initialized. Then a diabatic initialization, which includes surface drag, reduces ΔV_d by a factor of two in the lowest level. This result indicates that the balance in the small-scale, shallow modes is indeed diabatic, as described by Errico (1984) and Ballish and Baer (1985). If the surface drag term is excluded from the DIAB 9V-20T initialization, then the errors (not shown) are similar to those of the adiabatic case.

Values of horizontal-mean ΔV_d for the July dataset appear in Fig. 7c for the same initializations as in Fig. 7a. Qualitatively, the figures are similar, except that, for the July dataset, the ADIAB initialization produces smaller errors than does the FIXE-T initialization. Also, the spread between the errors from the various initializations is greater for the July case.

7. Analyses of mode coefficients

The only errors which have been examined thus far have been wind errors, and in particular, only divergent wind errors. Since the initializations are defined in terms of mode coefficients, it is appropriate to analyze errors in terms of the amplitudes themselves. The measure used here is the quantity R_l defined in Section 4.

The R_ls are evaluated over a subset of the gravitational modes for each equivalent depth. Table 3 shows the number of independent modes within each subset (there are 495 gravitational modes for each equivalent depth). Fig. 8 shows the ratio of the variances contributed by a subset

Table 3. *The number of modes within each range of natural periods, for each vertical mode index*

T (hours)	$l = 1$	2	3	4	5	6	7	8	9
[0,24]	494	492	483	441	352	290	270	262	262
[24,48]	1	2	10	45	124	136	132	128	124
[48,∞]	0	1	2	9	19	69	93	105	109

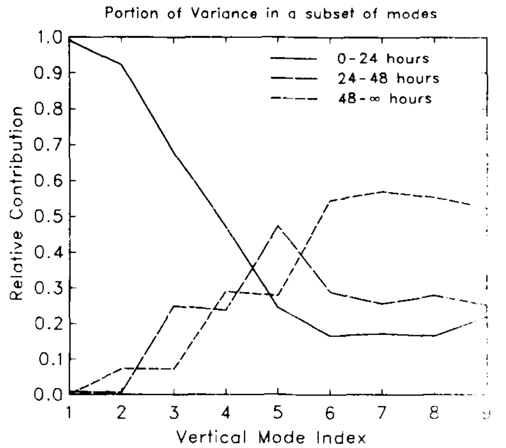

Fig. 8. The variance contributed by various sets of modes as a function of vertical mode index for January TRUTH.

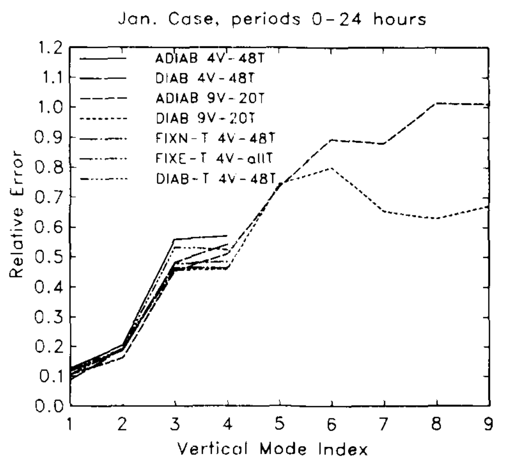

Fig. 9. R_l for high-frequency gravity modes for the January cases.

compared with that by all 495 modes for the January TRUTH.

The impact of the various NMIs on the faster waves of the January dataset are shown in Fig. 9.

For the four vertical mode initializations, R_l is evaluated only for the sets of modes with $T \leqslant 24$ hours. For any subset of modes, values of $R_l \geqslant 1$ imply no skill to a nonlinear normal-mode initialization. For $l = 1, \ldots, 4$, all the initialization produce similar results. For $l = 1$, $0.11 < R < 0.14$. This is the magnitude of error one may expect from attempting to replace the prognostic equations for these gravity-mode amplitudes by Machenhauer balance equations (see Section 8, or Errico, 1984). These errors are sufficiently small for many purposes, including for that of forecasting. For $l = 2$, the errors are less than 20%, which are still small. However, for $l = 3, 4$, the errors lie between 43% and 57%. These latter errors may be significant, depending on the purpose of the initialization.

The ADIAB and DIAB 9V-20T initializations are also included in Fig. 9. For these, the sets of modes evaluated are further restricted to those with $T \leqslant 20$ hours, although this is not indicated in the figure. If this restriction were not made, R_l would be misleadingly smaller since, in its evaluation, the denominator would include more modes, but the numerator would be unchanged. For $l = 1, \ldots, 4$, the results are not significantly different from those previously. However, these two initializations affect shallow modes, unlike those previously. For $l = 8, 9$, $R \approx 1$ for the adiabatic case. Correspondingly, $R \approx 0.65$ for the diabatic case. This is a further demonstration that the dynamic balance at the surface involves diabatic forces (Errico, 1983; Ballish and Baer, 1985).

Errors R_l from five initializations are compared in Fig. 10. The set of modes evaluated include only those with $24 \leqslant T \leqslant 48$ hours. For these modes the initializations show little or no skill. For $l = 1, 2$ there are only a few modes, and less than 10% of the variance is represented. Therefore corresponding values of R_l may change significantly for other cases. However, for $l = 3, 4$, several modes are averaged in the value of R, and those modes describe a significant portion of the total variance. The DIAB initializations show the most error. For $l = 4$, the FIXN and FIXE initializations with correct heating do better, although the error is still 80%.

The FIXE-T initializations include modes with $T > 48$ hours. For the January dataset, these modes contribute 7% of the variance for $l = 2, 3$ but 29% of the variance for $l = 4$. For all, the errors are greater than 90% (not shown). Interestingly, for these modes, the FIXE initialization with the correct heating does slightly worse than with the degraded heating. Much of the error can be attributed to phase differences between the true and initialized coefficients.

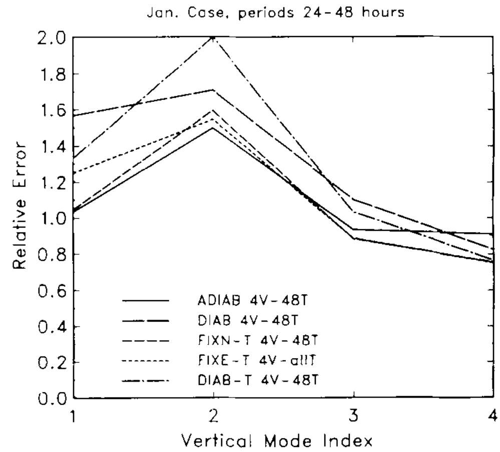

Fig. 10. R_l for low-frequency gravity modes for the January cases.

The corresponding results for the July case are shown in Figs. 11 through 13. The results are similar. The DIAB 9V-20T error is less for $l = 8, 9$, but for $l = 4$ most errors are slightly worse.

Fig. 13 is the July equivalent of Fig. 10. It shows small errors for $l = 1$ for some initializations, in contrast to Fig. 10. However that subset of modes includes only one member. For $l = 2, 3, 4$, the errors are generally less for the July case compared with the January case. This was observed in the errors of the V_d and ψ fields as well, and may be related to the fact that the July circulation is weaker than the January one.

For those modes with $T > 48$ hours in the FIXE initializations of the July dataset, the relative errors for the $l = 2, 3$ modes are greater than 140%, with either the correct or degraded heating fields. For $l = 4$, the errors for both are greater than 55%. This is smaller than for the January case, but still not insignificant.

In summary, for $l = 1, 2$, all the initializations do quite well. If the rotational mode amplitudes are known precisely, it is possible to determine the gravity mode amplitudes within 20% of their true values for these large vertical scales. For

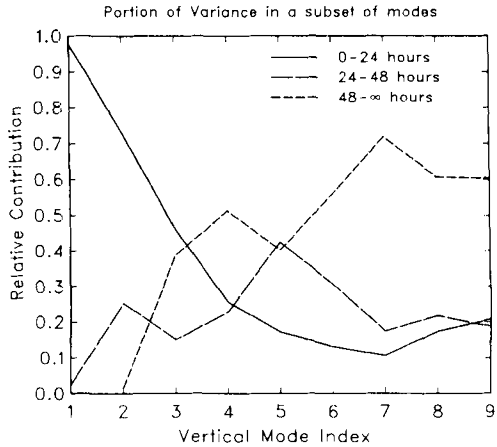

Fig. 11. As in Fig. 8 except for the July cases.

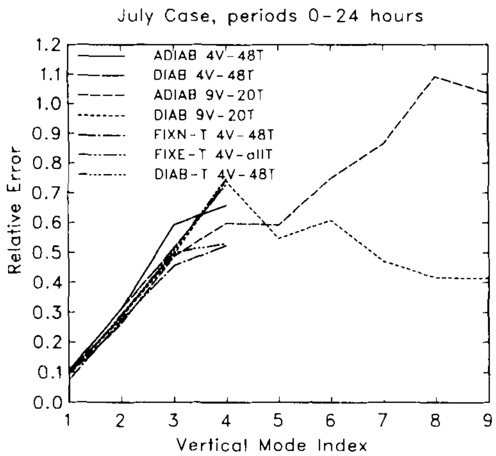

Fig. 12. As in Fig. 9 except for the July cases.

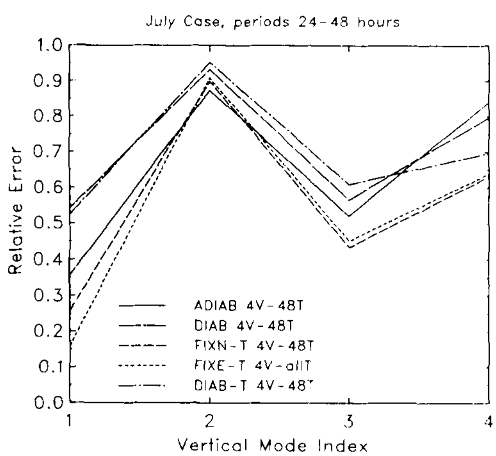

Fig. 13. As in Fig. 10 except for the July cases.

these modes, it makes little impact whether the initialization is diabatic or adiabatic. For $l = 3, 4$, all the initializations perform poorly. For the subset of modes whose natural periods are less than 1 day at these depths, the errors are between 40% and 50%. Diabatic initialization with correct heating produces an only slightly better result than adiabatic initialization when applied to these modes. However, the errors are near 100% for the naturally slower modes ($T > 24$ hours). For these modes there is no significant improvement with diabatic initialization. The modes whose amplitudes are significantly improved by diabatic initialization are the most shallow ones, which are strongly affected by strong surface processes. All these results will be explained in terms of a fundamental theory in Section 8.

8. Examination of mode equations

The results that have been presented are most easily explained by examining the prognostic equations for the mode amplitudes. For this purpose, the equations need not be considered in their full complexity. Instead, it is sufficient to consider the equation for a single mode, in the form

$$\frac{dc}{dt} = -(i\lambda + \nu)c + A(t) + D(t), \tag{8.1}$$

where t is time, λ is the mode's natural frequency (i.e., the eigenvalue associated with the mode), ν is a linear damping coefficient, i is $\sqrt{-1}$, and A and D represent all the other adiabatic and diabatic terms, respectively. To understand the behavior of c in the present context, it is sufficient to let $A + D$ have the simple form

$$A(t) + D(t) = (A(0) + D(0))\,e^{-i\mu t}. \tag{8.2}$$

The linear damping term is explicitly included in (8.1), since a damping mechanism is necessary to remove gravity waves (Errico, 1981) and otherwise singularities occur at resonance ($\mu = \lambda$).

Equation 8.1 is that for a simple, forced and damped harmonic oscillator. With the harmonic forcing given by (8.2), the general solution for c is

$$c(t) = \left[c(t_0) - \frac{A(t_0) + D(t_0)}{i\lambda - i\mu + \nu}\right] e^{-(i\lambda + \nu)(t - t_0)} + \frac{A(t) + D(t)}{i\lambda - i\mu + \nu}, \tag{8.3}$$

where t_0 may be any particular time. The term in brackets defines the "fast" part of the solution. It depends on some, as yet, unspecified value $c(t_0)$. For the model solution which we have labeled as TRUTH, dissipation mechanisms have had sufficient time to damp any initial gravity waves. The corresponding solution for (8.1) is

$$c_T(t) = \lim_{t - t_0 \to \infty} c(t) = \frac{A(t) + D(t)}{i\lambda - i\mu + \nu}. \tag{8.4}$$

Note that for this solution, the mode coefficient has the time scale of the forcing (μ), and not its natural time scale (λ). For a diabatic initialization, c is determined from the solution of (8.1) with the time tendency term; (i.e., the left hand side) set to zero. The result is

$$c_D(t) = \frac{A(t) + D(t)}{i\lambda + \nu}. \tag{8.5}$$

For an adiabatic initialization, both D and ν are also neglected, to yield

$$c_A(t) = \frac{A(t)}{i\lambda}. \tag{8.6}$$

The normalized error due to replacing c_T by c_D, evaluated as in (4.6), is

$$R_D = |\mu|/(\lambda^2 + \nu^2)^{1/2}. \tag{8.7}$$

Except for the shallowest modes, ν can usually be neglected compared with λ, so that

$$R_D \approx |\mu/\lambda|. \tag{8.8}$$

Therefore, the relative error in assuming diabatic balance is small only if the forcing frequency is much less than the mode's natural frequency. Equivalently, the time tendency term is negligible compared to the linear term only if this frequency relationship is true.

The normalized error due to replacing c_T by c_A is

$$R_A = \left| \frac{[(\mu - i\nu)/\lambda] A + D}{A + D} \right|. \tag{8.9}$$

If the diabatic terms are small compared to the adiabatic terms, then R_A appears as R_D in (8.8). However, if D dominates A, then $R_A \approx 1$. Simply, if any large term is neglected in the initialization procedure, the initialized amplitudes will be significantly different from the true amplitudes. This applies not only if the large term is a diabatic one, but also if it is the time-tendency term.

In the case of external gravitational modes, $|\lambda|$ is so large, and A dominates D so greatly that R_A is small (Errico, 1984). However, the result is very different for those gravitational modes which describe most large-scale features of the tropical circulation. In particular, this set includes the low wave-number, $l = 4$, Kelvin modes (Puri, 1983). These modes have natural periods between one and 14 days. The relative errors due to initialization will be small only if the advection and diabatic heating act as forces with characteristic periods significantly longer than this. In the CFM, Fig. 8 in Errico (1984) indicates that the diabatic forcing on these modes is approximately 50% larger than the adiabatic forcing due to rotational modes (i.e., due to quasi-rotational dynamics). However, the power-weighted, mean frequency of these tropical gravitational modes is approximately 1.3×10^{-5} s^{-1}, corresponding to a mean period of 5.6 days. This suggests that the frequencies of their significant forcing mechanisms are close to their natural frequencies, so that the gravity-wave behavior is maintained in the presence of dissipation.

9. Conclusions and discussion

Several different initialization schemes were applied to simulated January and July datasets. When analyzed in terms of zonal-mean meridional mass streamfunctions, the results were similar to those reported elsewhere (Rasch, 1985; Puri, 1983, 1985; Puri and Bourke, 1982; Kitadi, 1983; Bengtsson, 1981; Wergen, 1983). Adiabatic schemes weakened the zonal-mean circulations. Diabatic schemes over-strengthened them. Schemes which used time averaged heating produced smaller changes than either the adiabatic or diabatic with instantaneous heating profiles. This may be due in part to the exclusion of some of the diabatic processes as listed in Section 3. Errors due to the initializations could be further limited by restricting the set of modes initialized to exclude those which described most of the zonal-mean circulation. These conclusions specifically apply to zonal wavenumber zero only.

In order to examine the nonzonal results, errors in the divergent component of the velocity field were examined. All the initializations produced substantial errors in the tropics. This was less apparent from a simple comparison of velocity potential fields. As for the previous diagnostic, the schemes which used time averaged heating, or which more severely restricted the set of modes affected, produced the best results, although the qualitative differences between most schemes were not large. An important exception was that, when applied to all vertical modes, a diabatic scheme which included surface drag produced much smaller errors at the surface than a corresponding adiabatic scheme. However, the variances of the errors in the wind divergence in the tropics were approximately 50% of the true divergent wind variance for almost all the schemes (including the schemes which used time averaged heating as a diabatic term).

The results of the various schemes were succinctly summarized by presentation of the changes in normal mode coefficients produced by each scheme. This was most appropriate because all the schemes were formulated in terms of normal modes. In this way, the results were easily stratified in terms of vertical and horizontal scales, although the latter was actually discussed in terms of corresponding natural periods. The largest vertical, but smallest horizontal scales were better initialized (errors were typically 10%) than the medium or smaller depth, large scale modes (with errors greater than 80%).

Most of the above results were explained in terms of a pedagogic prognostic equation for a single mode amplitude. The errors due to various initialization schemes were shown to depend not only on improper specification of forces (such as ignoring diabatic processes), but also on ignoring the amplitude's time tendency; i.e., the Machenhauer balance condition is not appropriate for most internal modes. It is possible that some higher-order balance condition (in which the time tendencies are not ignored; Tribbia, 1984) is appropriate for these modes. However, this possibility was not explored in this study.

The most important conclusion from this study is that the inclusion of convective heating in a normal mode initialization scheme does not greatly improve the initial field specifications compared with corresponding adiabatic schemes. The reason for this lack of improvement is simply that the modes which are predominant in the tropics have natural periods which are not much different than the time scales of the various diabatic and adiabatic processes which force the modes. The time-tendencies of the modes are not negligible compared with other terms in the equations. The heating is a transient process that excites tropical modes which may then propagate freely. As with the rotational modes, these modes are appropriately described by prognostic, rather than diagnostic (i.e., balanced) equations. These conclusions agree with Errico's (1984) analysis of dynamic balance in the simulation model used, and with the analytic results of Silva Dias et al. (1983).

There is another difficulty with using convective heating in normal mode initialization. Initialization is required because the portions of the fields described by gravitational modes are poorly analyzed. If determination of the convective heating depends on these portions of the fields, (e.g., the convection depends upon the divergence field) then the convective heating will also be determined poorly. In this case, even if the parameterization of convection were very realistic, the heating field would still be inaccurate. By initialization, we are attempting to recompute the fields described by the gravitational modes. It seems unlikely that an initialization produced from such heating can result in much more accurate fields, given the sources of error in each step of the process.

The easiest way to limit changes to an analysis by an initialization is to restrict the set of modes affected. For example, if changes to the zonal-mean meridional circulation are not desired, one can simply not initialize any zonal-mean modes. The ability to be scale selective is one of the advantages of normal mode schemes compared with local schemes. However, it is possible that by excluding some set of modes, the forecast is much noisier than desired. The user must decide how much he wants to retain the analysis, and what level of noise he will permit. These are some of the questions regarding normal mode initialization that still need exploration.

The result that diabatic NMI shows only a limited improvement compared to adiabatic NMI appears discouraging. However, it is important to note that even when all data regarding most fast gravitational modes are absent (as after the linear NMI performed for the experiments), either type of nonlinear NMI is able to reasonably reproduce the original data. Also, where the reproductions produce large errors (e.g., in the tropics), those errors are nowhere much larger than the magnitudes of the true fields. So, NMI may yield information (perhaps spectra) regarding poorly analyzed fields, even in cases where a point-by-point measure of usefulness is small.

The conclusions of this study are unavoidably model-dependent. The most significant results concern the circulation in the tropics. This is one of the areas most sensitive to diabatic processes and therefore to model-dependent parameterization schemes. It is also the area where most models consistently show little forecast skill (e.g., Heckley, 1985). It is strongly recommended that similar studies be done with other models in order to determine the generality of these results.

A critical question is: What is the partitioning between transient and quasi-stationary activity of the large-scale, internal gravitational modes in the tropical atmosphere. If these modes have a substantial transient component, then a Machenhauer (1977) type balance would be as unsuitable for a true state as it is for the CFM simulated states. Conversely, if a strong quasi-stationary component exists, then some type of balance condition may be appropriate. Regarding this point, it must be stressed that the distinction between transience and quasi-stationarity varies from mode to mode, depending on their natural frequencies. A slow variation over 5 to 10 days illustrates stationarity for one mode, but transience for another (e.g., for an internal Kelvin mode).

Characteristics of the CFM tropical simulations are presented in Williamson and Williamson (1984). None of these reported characteristics can be used to determine the time-scale partitioning in the model simulations. Neither is it possible to do so for the atmosphere from the usual presented statistics (e.g., those in Lau, 1984). The usual time and space averaging, and the non-separation of rotational from gravitational modes, makes the indirect determination of this partitioning difficult, if not impossible.

No χ fields are presented in Williamson and Williamson (1984). Therefore, 30-day time-mean fields of χ at 200 and 850 mb determined from days 61–90 of the perpetual January simulation are presented in Figs. 14a, b. These may be compared with monthly-mean χ fields determined from version 3b of the analyses for January of the year of the First GARP (Global Atmospheric Research Program) Global Experiment (FGGE-3b) produced at the Geophysical Fluid Dynamics Laboratory (GFDL) and, independently, at ECMWF which are presented in Lau (1984). They may also be compared with monthly-mean χ fields determined for January 1983 produced at the National Meteorological Center (NMC) and at ECMWF which are presented by Rosen and Salstein (1985). Close agreement with any of these analysis cannot be expected since the CCM0B has been used to simulate the climate and not to make a forecast for these same Januaries. However, both the magnitudes and locations of extrema are qualitatively not unlike those of the analyses considering the differences between the analyses themselves. These similarities indicate that, for the purposes of this study, the CFM produces a monthly-mean component of the tropical divergence not significantly unlike that of the atmosphere. For comparison of other fields with atmospheric analyses, the reader should compare Williamson and Williamson (1984) with Lau (1984).

It would be extremely useful if the characteristics of Kelvin modes in the CFM simulations could be compared with observed atmospheric characteristics. However, the divergence fields which describe these modes have been too poorly analyzed to date (Julian, 1983; Daley, 1983; Daley and Mayer, 1986). Comparison of analyses produced at GFDL and ECMWF for FGGE, when tropical observations were most abundant, indicates that even the large-scale quasi-stationary component of the divergence field has been poorly analyzed (see Lau, 1984). Differences between corresponding, analyzed monthly-mean velocity potential fields are nearly as large as the ECMWF analyzed values in many places. Therefore, any model comparisons with these analyzed data must carefully consider the data quality. It appears that the current observation and analysis system is inadequate for determining the time-scale partitioning of Kelvin modes. Perhaps other, indirect methods (e.g., station time-series analysis as done by Nitta et al., 1986) can be used

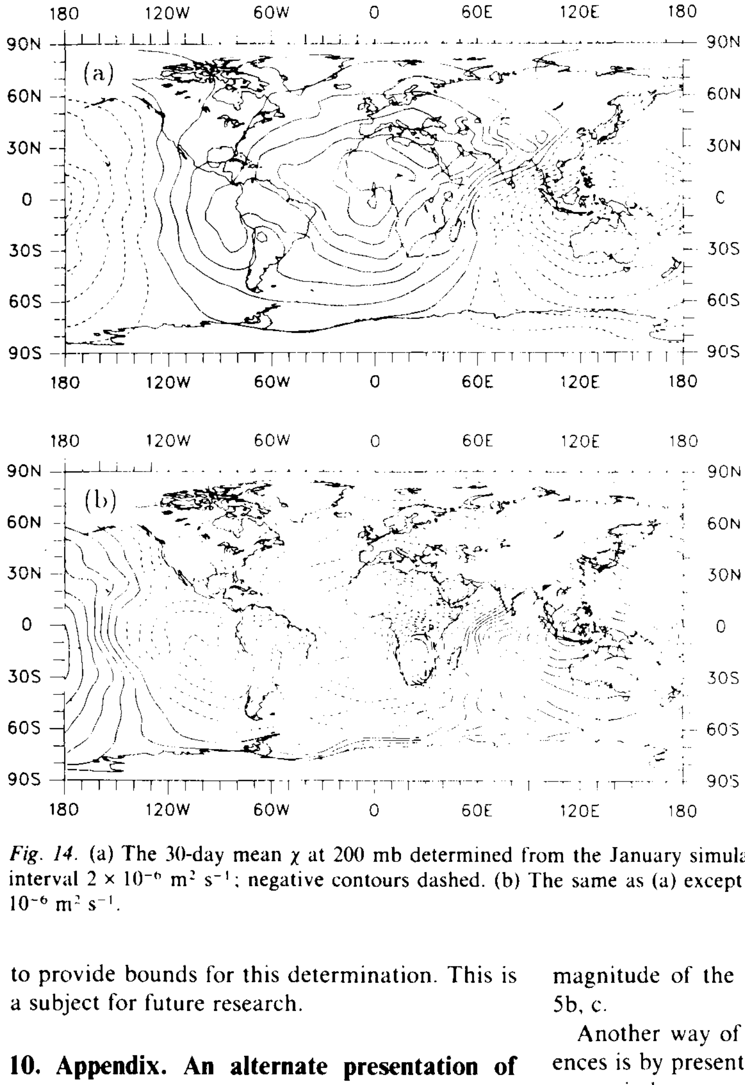

Fig. 14. (a) The 30-day mean χ at 200 mb determined from the January simulation centered at day 75. Contour interval 2×10^{-6} m^2 s^{-1}; negative contours dashed. (b) The same as (a) except at 850 mb, with contour interval 10^{-6} m^2 s^{-1}.

to provide bounds for this determination. This is a subject for future research.

10. Appendix. An alternate presentation of the divergent winds

In order to compare the appropriateness of presenting figures of magnitudes of velocity differences (Figs. 5a–c) with those of χ fields, Figs. 15a–c are presented here, as requested by a reviewer. These are the χ fields at $\sigma = 0.189$ for the January case determined by TRUTH, ADIAB 4V-48T, and FIXN-T 4V-48T, respectively. It appears from these figures that both initialized fields are smoother than that of TRUTH, and that the adiabatic initialized field is smoothest. However, careful consideration of gradients is required in order to determine the magnitude of the differences presented in Figs. 5b, c.

Another way of presenting the velocity differences is by presenting figures of the vector divergent winds corresponding to Figs. 15a–c. These are presented in Figs. 16a–c, respectively. If only magnitudes of differences are of interest, and not the directions of the actual winds, then Figs. 5b, c are appropriate since for them it is unnecessary for the reader to perform the vector subtraction required for Figs. 16a–c. Of course, some particular information regarding the wind fields cannot be determined from Figs. 5a–c, but can be determined from Figs. 15–16. However, since such information is not apparently relevant in the present context, while the magnitudes of the differences are entirely relevant, the presentations of Figs. 5a–c are more appropriate.

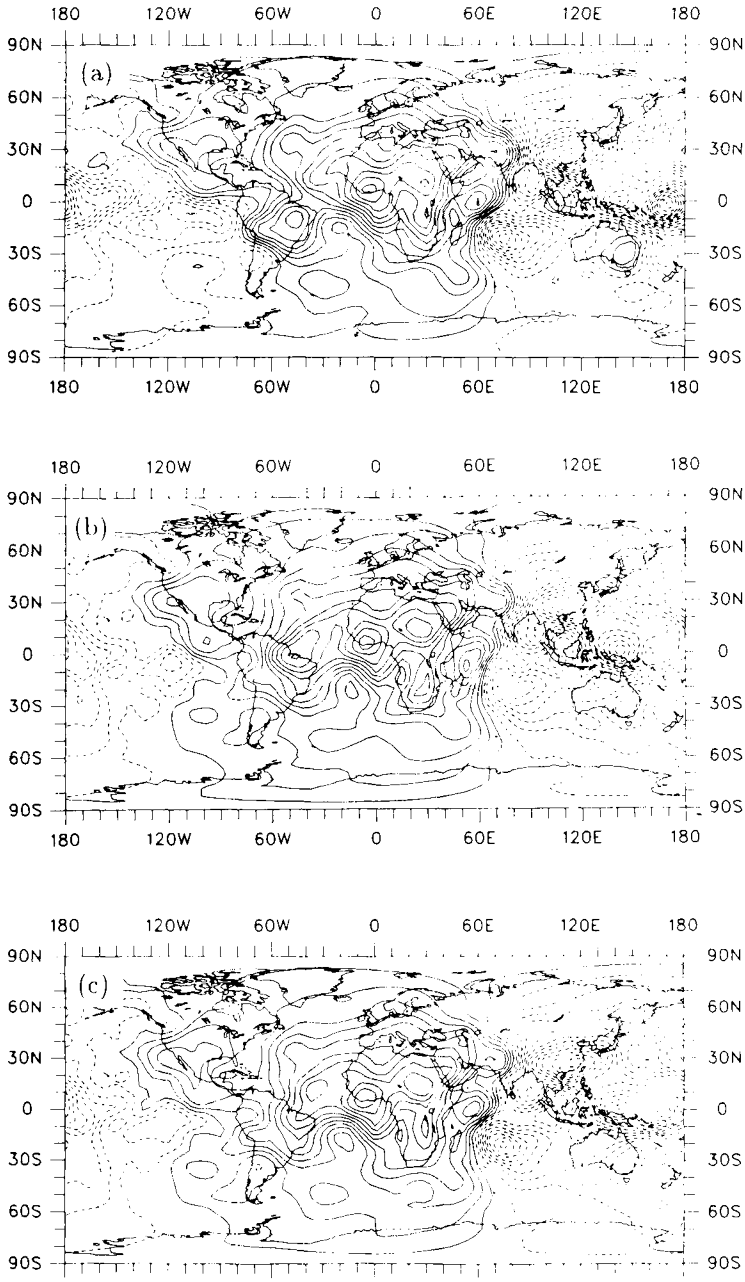

Fig. 15. The χ fields at $\sigma = 0.189$ for (a) TRUTH, (b) ADIAB 4V-48T, and (c) FIXN-T 4V-48T. Contour interval 2×10^{-6} m^2 s^{-1}; negative contours dashed.

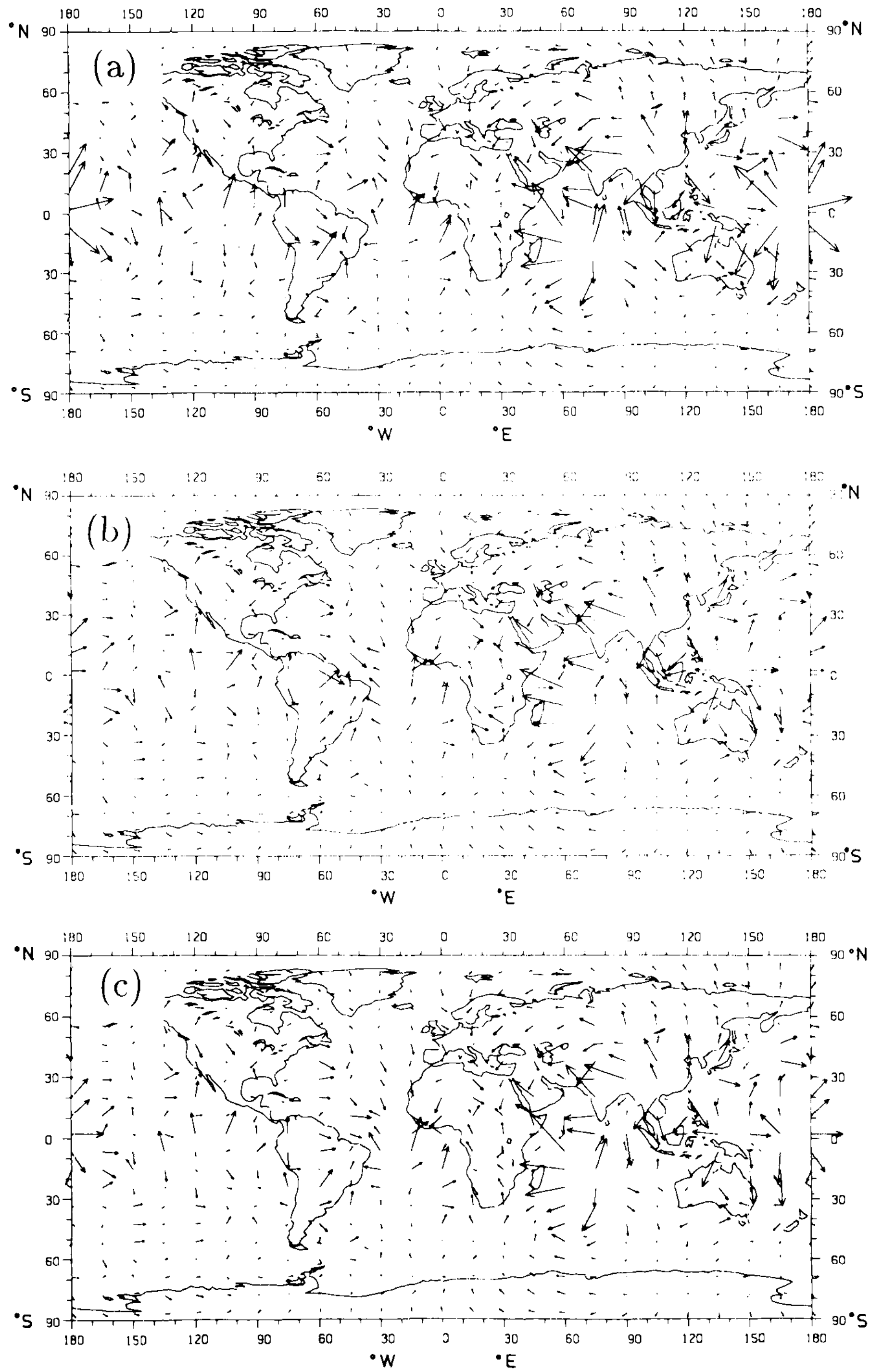

Fig. 16. Vectors of divergent wind corresponding to respective χ fields in Fig. 15a–c. Values at every other model grid point are indicated. The distance between indicated points corresponds to a speed of 10 m s^{-1}.

11. Acknowledgements

We thank D. Baumhefner, A. Kasahara, and J. Tribbia for their comments on the manuscript, and those colleagues plus R. Daley and D. Williamson for their many suggestions during the course of this work. We also thank B. Ballish and W. Wergen for their explanation of the initialization methods used at NMC and ECMWF, respectively. This work was partially funded by U.S. Navy Grant No. NA6685684WR84018, and performed at the National Center for Atmospheric Research, which is sponsored by the National Science Foundation.

REFERENCES

Baer, F. 1977. Adjustments of initial conditions required to suppress gravity oscillations in nonlinear flows. *Contrib. Atmos. Phys. 50*, 350–366.

Ballish, B. A. and Baer, F. 1985. Normal mode initialization with elementary surface friction. *Mon. Wea. Rev. 113*, 241–247.

Bengtsson, L. 1975. Four-dimensional assimilation of meteorological observations. *GARP Publication Series, No. 15*, WMO, 76 pp. [Available from UNIPUB, New York, NY 10010, U.S.A.]

Bengtsson, L. 1981. Current problems in four-dimensional data assimilation. *Data Assimilation Methods, ECMWF Seminar 1980*, 195–217. [Available from the European Centre for Medium Range Weather Forecasts, Shinfield Park, Reading RG2 9AX, England.]

Daley, R. 1985. The analysis of synoptic scale divergence by a statistical interpolation procedure. *Mon. Wea. Rev. 113*, 1066–1079.

Daley, R. and Mayer, T. 1986. Estimates of global analysis errors from the Global Weather Experiment observational network. *Mon. Wea. Rev. 114*, 1642–1653.

Errico, R. M. 1981. An analysis of interactions between geostrophic and ageostrophic modes in a simple model. *J. Atmos. Sci. 38*, 544–553.

Errico, R. M. 1983. Convergence properties of Machenhauer's initialization scheme. *Mon. Wea. Rev. 111*, 2214–2223.

Errico, R. M. 1984. The dynamical balance of a general circulation model. *Mon. Wea. Rev. 112*, 2439–2454.

Heckley, W. A. 1985. Systematic errors of the ECMWF operational forecasting model in tropical regions. *Q. J. R. Meteorol. Soc. 111*, 709–738.

Julian, P. R. 1985. Some comparisons of ECMWF IIIb and GFDL IIIb analyses in the tropics. *Proc. First National Workshop on the Global Weather Experiment*, Vol. II, Part 1. National Academy Press, Washington, D.C., U.S.A., 211–216.

Kanamitsu, M. 1985. *A study of the predictability of the ECMWF operational forecast model in the tropics.* ECMWF Technical report No. 49, 77 pp. [Available from the European Centre for Medium Range Weather Forecasts, Shinfield Park, Reading RG2 9AX, England.]

Kasahara, A. 1978. Further studies on a spectral model of the global barotropic primitive equations with Hough harmonic expansions. *J. Atmos. Sci. 35*, 2043–2051.

Kitadi, T. 1983. Nonlinear normal mode initialization with physics. *Mon. Wea. Rev. 111*, 2194–2213.

Krishnamurti, T. N., Pasch, R. J., Pan, H. L., Chu, S. H. and Ingles, K. 1983. Detail of low latitude medium range numerical weather prediction using a global spectral model. I: Formation of a monsoon depression. *J. Meteorol. Soc. Japan 61*, 188–207.

Lau, N.-C. 1984. *A comparison of the circulation statistics based on FGGE level III-B analyses produced by GFDL and ECMWF for the special observation periods.* NOAA Data Report ERL GFDL-6, 237 pp. [Available from Geophysical Fluid Dynamics Laboratory, P.O. Box 308, Princeton, NJ 08542, U.S.A.]

Lorenz, E. N. 1967. *The nature and theory of the general circulation of the atmosphere.* WMO Publication No. 218, 161 pp.

Machenhauer, B. 1977. On the dynamics of gravity oscillations in a shallow water model with applications to normal mode initialization. *Contrib. Atmos. Phys. 50*, 253–271.

Machenhauer, B. 1979. The spectral method. *Numerical Methods Used in Atmospheric Sciences*, Vol. II, GARP Publication Series No. 17, WMO, 124–277. [Available from UNIPUB, New York, NY 10010, U.S.A.]

Nitta, T., Nakagomi, Y., Suzuki, Y., Hasegawa, N. and Kadokura, A. 1985. Global analysis of the lower tropospheric disturbances in the tropics during the northern summer of the FGGE year. Part I: Global features of the disturbances. *J. Meteorol. Soc. Japan 63*, 1–19.

Puri, K. 1983. The relationship between convective adjustment, Hadley circulation, and normal modes of the ANMRC spectral model. *Mon. Wea. Rev. 111*, 23–33.

Puri, K. 1985. Sensitivity of low-latitude velocity potential field in a numerical weather prediction model to initial conditions, initialization and physical processes. *Mon. Wea. Rev. 113*, 449–466.

Puri, K. and Bourke, W. 1982. A scheme to retain the Hadley circulation during nonlinear normal mode initialization. *Mon. Wea. Rev. 110*, 327-335.

Ramanathan, V., Pitcher, E. J., Malone, R. C. and Blackmon, M. L. 1983. The response of a spectral general circulation model to refinements in radiative processes. *J. Atmos. Sci. 40*, 605–630.

Rasch, P. J. 1985. Developments in normal mode initialization, Part II: A new method and its comparison with currently used schemes. *Mon. Wea. Rev. 113*, 1753–1770.

Rosen, R. D. and Salstein, D. A. 1985. Effect of initialization on diagnoses of NMC large-scale circulation statistics. *Mon. Wea. Rev. 113*, 1321–1337.

Silva Dias, P. L., Shubert, W. and DeMaria, M. 1983. Large scale response of the tropical atmosphere to transient convection. *J. Atmos. Sci. 40*, 11, 2689–2707.

Tribbia, J. J. 1984. A simple scheme for high-order nonlinear normal-mode initialization. *Mon. Wea. Rev. 112*, 278–284.

Wergen, W. 1983. Initialisation. Interpretation of Numerical Weather Prediction Products, ECMWF Seminar/Workshop 1982, 31–57. [Available from the European Centre for Medium Range Weather Forecasts, Shinfield Park, Reading RG2 9AX, England.]

Williamson, D. L. 1983. Description of the NCAR Community Climate Model (CCM0B). NCAR Tech. Note TN-210+STR, 93 pp. [NTIS No. PB83-231068.]

Williamson, D. L. and Temperton, C. 1981. Normal mode initialization for a multilevel grid-point model, Part II: Nonlinear aspects. *Mon. Wea. Rev. 109*, 744–757.

Williamson, D. L. and Williamson, G. S. 1984. Circulation statistics from January and July simulation with the NCAR Community Climate Model (CCM0B). NCAR Technical Note TN-244+STR, 112 pp. [Available from the National Center for Atmospheric Research, P.O. Box 3000, Boulder, CO 80307, U.S.A.]